하이브리드 레벨 셋을 이용한 이미지 분할

주기세* · 김은석**

Image segmentation Using Hybrid Level Set

Ki-See Joo* · Eun-Seok Kim**

요 약

기존의 레벨셋을 이용한 이미지 분할 방법은 화소값의 기울기를 이용하기 때문에 지역적 형태에 좌우되는 문제점을 지니고 있다.

본 논문에서는 평활한 구동력을 위하여 레벨 셋 함수와 새로운 보상 평활화 함수를 결합시키는 하이브리드 방법을 이용한 방법이 소개된다. 대부분의 경우에 3 교점을 가지고 있지 않다는 가정하에 보상함수를 얻는 방법을 대안으로 고려하였다. 보상함수의 주요 역할은 원보상 함수와 평균 보상함수의 차가 새로운 레벨셋 함수의 합리적인 구동력으로 소개될 수 있다.

본 논문에서 제안한 하이브리드 방법은 기존 레벨셋을 이용한 방법의 단점을 최소화시키는 방법이다.

ABSTRACT

The conventional image segmentation method using level set has been disadvantage since level set function in the gradient-based model evolves depending on the local profile of the edge.

In this paper, a new model is introduced by hybridizing level set formulation and complementary smooth function in order to smooth the driving force. We consider an alternative way of getting the complementary function(CF) which is much easier to simulate and makes sense for most cases having no triple junctions. The rule of thumb is that CF must be computed such that the difference between their average and the original CF function should be able to introduce a reliable driving force for the evolution of the level set function.

This proposed hybrid method tries to minimize drawbacks the conventional level set method.

키워드

gradient-based model, complementary smooth function, hybridizing level set, driving force

Ⅰ. Introduction

In this article, we develop efficient numerical algorithms for the level set segmentation, combining the following two level in following two level set methods:

- gradient-based method studied by Zhao at al. [21], and
- gradient-tree method of Chan and Vese [3,4], which is developed from the Mumford-Shah functional in image processing [13]. They turn out to allow researchers not only to introduce innovative

*목포해양대학교 해양운송시스템학부

**아주대학교 산업공학과

접수일자 : 2004. 10. 29

mathematical models but also to analyze and improve traditional algorithms.

we consider preliminaries, beginning with general remarks for segmentation. Then we visit briefly the level set models, such as the gradient-based model [21] (see also [1, 2, 10, 11]) and the Mumford-Shah functional in image processing [3, 4, 13]. The next section presents a hybrid method, combining there two methods, which tries to minimize drawbacks from both sides.

1.1 General remarks

For a given image u^0, we denote the desired contours of edges by Γ. When a level set function $\phi : \Omega \rightarrow \mathbb{R}$[15] is incorporated with a segmentation method, the contours of edges are identified by the zero-level set, i.e.,

$$\Gamma = \{ x : \phi(x) = 0\}$$

Changes in values of the level set function can reform the contours of the desired edges. Such mathematical techniques are called the methods of acting contours or snakes. Effectiveness and efficiency of the snake methods depend strongly on a complementary function (CF) of u^0, which we define in this article as a function that invokes the driving force for the level set function ϕ. The CF must be incorporated in such a way that it is easy to compute and introduces a reliable driving force for the change of the level set function and therefore the zero-level set.

For instance, see Figure 1, where the solid curve indicates the given image u^0 and the dashed curve is an initial guess for the level set function ϕ. The desired zero-level set consists of two points that are denoted by bullets X_i, i = 1,2 and the current zero-level set is the points P_i i = 1,2. Assume that a CF is computed such that the corresponding driving force for the level set function be negative near P_1 and positive near P_2. Then, it is clear to see that P_1 and P_2 are getting closer to X_1 and X_2, respectively. Thus it is very important to compute an effective representation of u^0 in order to invoke such a reliable driving force for the level set function.

We will back to this issue later when we consider acceleration techniques in §4.

1.2 Gradient-based segmentation

There are lots of classical contour models. Among other, we consider the variational level set formulation of Zhao *etal.* [21]:

$$\begin{aligned} \phi_t &= |\nabla\phi| \nabla \cdot \left(g \frac{\nabla\phi}{|\nabla\phi|} \right) \\ &= |\nabla\phi| \left(g k_\phi + \nabla g \cdot \frac{\nabla\phi}{|\nabla\phi|} \right) \\ &= |\nabla\phi| g k_\phi + \nabla g \cdot \nabla\phi \end{aligned} \tag{1.1}$$

where $k_\phi := \nabla \cdot (\nabla\phi / |\nabla\phi|)$, the mean curvature. The edge detector $g = g(\nabla u^0)$ is defined as, for some $\zeta > 0$ and $p \geq 1$,

$$g(\nabla u^0) = \frac{1}{\zeta + |J * \nabla u^0|^p} \tag{1.2}$$

where J is a Gaussian of variance σ

The driving force inherited in the segmentation model (1.1) can be summarized as follows:

- Motion with normal velocity, which is equal to its curvature times the edge detector. (This component of the force drives the contour smoother)
- Convection in the direction that is the gradient of the edge detector.

Note that the edge detector g plays the role of CF, which invokes a driving force for the level set function. It has been numerically verified that the choices of ζ, J, and p in g often become a crucial component in the performance of the model (1.1).

1.3 Mumford-Shah segmentation

The Mumford-Shah minimization for segmen-

tation [13] reads

$$\min_{\Gamma,u} E_{MS}(\Gamma,u) \tag{1.3}$$

where $E_{MS}(\Gamma,u) = \eta \cdot \text{length}(\Gamma) + \lambda \int_{\Omega} |u-u^0|^2 dx + \mu \int_{\Omega/\Gamma} |\nabla u|^2 dx$ (1.4)

Here Ω denotes the domain for the image, η, λ, and μ are nonnegative constants, and u is a CF that is locally smooth except near Γ.

To present the level set formulation proposed in [3,4], we first consider the Heaviside function H (in the one-dimensional space) defined by

$$H(\xi) = \begin{cases} 1, & \text{if } \xi \geq 0 \\ 0, & \text{if } \xi < 0 \end{cases}$$

Define the CF u as

$$u(X) = u^+(X)H(\phi(X)) + u^-(X)(1-H(\phi(X))) \tag{1.5}$$

Where u^+ and u^- are two C^1 functions that are to be updated during the simulation. Note that the CF u can be identified by u^+ and u^-, i.e.,

$$u(X) = \begin{cases} u^+(X), & \text{if } X \in \Omega_\phi^+ := \{X | \phi(X) > 0\} \\ u^-(X), & \text{if } X \in \Omega_\phi^- := \{X | \phi(X) < 0\} \end{cases}$$

Then, the Mumford-Shah functional (1.4) can be rewritten as (λ=1)

$$\begin{aligned} E_{MS}(u^+,u^-,\phi) &= \eta \int_{\Omega} |\nabla H(\phi)| dx \\ &+ \int_{\Omega} |u^+ - u^0|^2 H(\phi(X)) dx \\ &+ \int_{\Omega} |u^- - u^0|^2 (1-H(\phi(X))) dx \\ &+ \mu \int_{\Omega} |\nabla u^+|^2 H(\phi(X)) dx \\ &+ \mu \int_{\Omega} |\nabla u^-|^2 (1-H(\phi(X))) dx \end{aligned} \tag{1.6}$$

where we have utilized the following identity

$$\text{length}(\Gamma) = \int_{\Omega} |\nabla H(\phi)| dx$$

It is not difficult to find the associated Euler-Lagrange (EL) equations For u^+, u^-, and ϕ, by utilizing mathematical techniques in the calculus of variations [18]; see also [3,4]. The EL equation for ϕ is $\frac{\partial \phi}{\partial t} =$

$$\begin{aligned} &\delta_\epsilon(\phi)\left[\eta \nabla \cdot \left(\frac{\nabla \phi}{|\nabla \phi|}\right) - (u^+ - u^0)^2 + (u^- - u^0)^2\right] \\ &+ \delta_\epsilon(\phi)\left[-\mu |\nabla u^+|^2 + \mu |\nabla u^-|^2\right] \\ &= \delta_\epsilon(\phi)\left[\eta \nabla \cdot \left(\frac{\nabla \phi}{|\nabla \phi|}\right) - 2(u^+ - u^-)\left(u^0 - \frac{u^+ + u^-}{2}\right)\right] \\ &\quad + \delta_\epsilon(\phi)\left[-\mu |\nabla u^+|^2 + \mu |\nabla u^-|^2\right] \end{aligned} \tag{1.7}$$

and the EL equations for u^+ and u^- are

$$\begin{aligned} &\text{(a)} \quad u^+ - u^0 = \mu \Delta u^+, \; X \in \Omega_\phi^+ \\ &\text{(b)} \quad u^- - u^0 = \mu \Delta u^-, \; X \in \Omega_\phi^- \end{aligned} \tag{1.8}$$

where η denotes the unit normal and δ_ϵ is an approximation of the Dirac function (the derivative of an approximate Heaviside function [3]) defined as

$$\begin{aligned} \delta_\epsilon(\xi) &= \frac{d}{d\xi} H_\epsilon(\xi) \\ &= \frac{d}{d\xi}\left[\frac{1}{2} + \frac{1}{\pi} \tan^{-1}\left(\frac{\xi}{\epsilon}\right)\right] = \frac{1}{\pi} \frac{\epsilon}{\epsilon^2 + \xi^2} \end{aligned} \tag{1.9}$$

where ϵ is a positive parameter.

The level set equation (1.7) can be simulated (as the time integration), with the solutions of the elliptic equations (1.8) incorporated in each time step. One can easily see that solving these elliptic problems (when an appropriate boundary condition is applied on $\{X | \phi(X) = 0\}$) is the most costly component of the simulation.

Note that the curvature term, $\eta \nabla \cdot (\nabla \phi / |\nabla \phi|)$ in (1.7), makes the level set function smoother as the parameter η grows. On the other hand, the difference between the image u^0 and the average of u^+ and u^- is an important component for the driving force for the level set function ϕ. Thus, the CF u (as a combination of u^+ and u^-) must be computed such that it can invoke an appropriate and reliable force for the evolution of the zero-level

set to the desired edges.

In the context, the Mumford-Shah- Chan-Vese (MSCV) model (1.7)-(1.8) shows two major drawbacks on (a) how to apply boundary condition for the elliptic differential equations and (b) how to extend $u^{\pm}$ to $\Omega_{\phi}^{\mp}$. Chan and Vese [3,4] suggested the no-flux boundary condition; for methods for the extension of $u^{\pm}$, see [CITES]. However, they work well for essentially binary (or piecewise constant) images but hardly make sense for segmenting general images.

When u^{+} and u^{-} are assumed constants, i.e. $u^{+} = C^{+}$ and $u^{-} = C^{-}$, one does not have to solve (1.8) explicitly and the EL equation (1.7) can be simplified as $\frac{\partial \phi}{\partial t}$ = (1.10)

$$\delta_{\epsilon}(\phi)\left[\eta\nabla\cdot\left(\frac{\nabla\phi}{|\nabla\phi|}\right)+2(C^{+}-C^{-})\left(u^{0}-\frac{C^{+}+C^{-}}{2}\right)\right]$$

where $C^{\pm}$ are averages of ϕ in $\Omega_{\phi}^{\pm}$ defined

$$\text{as}\quad C^{+}=C^{+}(\phi)=\frac{\int u^{0}(y)H(\phi(y))dy}{\int H(\phi(y))dy} \qquad (1.11)$$

$$C^{-}=C^{-}(\phi)=\frac{\int u^{0}(y)(1-H(\phi(y)))dy}{\int(1-H(\phi(y)))dy}$$

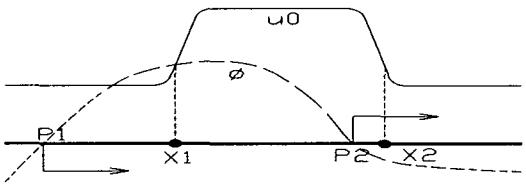

Figure 1. A given image (solid curve) and an initial guess for the level set function (dashed curve).

The segmentation algorithm utilizing the locally constant CF, (1.10)-(1.11), works for essentially binary images quite effectively. For example, consider the image and the level set function in Figure 1. It is apparent to see

$$\min_{x\in\Omega} u^{0}(x) \le C^{-} < C^{+} \le \max_{x\in\Omega} u^{0}(x)$$

and therefore

$$2(C^{+}-C^{-})\left(u^{0}(X)-\frac{C^{+}+C^{-}}{2}\right)$$

$$=\begin{cases} <0, & \text{if } X<X_1, \\ >0, & \text{if } X\in(X_1, X_2), \\ <0, & \text{if } X>X_2 \end{cases} \qquad (1.12)$$

Thus, the time integration with (1.10)-(1.11) would result in the zero-level set $\{P_1, P_2\}$ getting closer to the desired edges $\{X_1, X_2\}$.

III. The Model

In this section, we present a hybrid model, which combines the gradient-based model (1.1) and the MSCV model (1.7)-(1.8). Then, an efficient computational algorithm is considered for the model.

2.1 New hybrid model

We first note that the curvature term in (1.7) has the major role of the smoothing level set function, which can be replaced by as reasonable smoothing term. In the new model, we will substitute the right side of (1.1) for it. It also should be noticed that the terms involving $|\nabla u^{\pm}|$ have been introduced to make the CF smoother; they may be dropped as long as the CF is smooth enough.

Now, we explicitly define the hybrid model: for some $\alpha, \beta \ge 0$,

$$\frac{\partial\phi}{\partial t}-\alpha|\nabla\phi|\nabla\cdot\left(g\frac{\nabla\phi}{|\nabla\phi|}\right) \qquad (2.1)$$

$$=\beta\delta_{\epsilon}(\phi)[(u^{-}-u^{0})^{2}-(u^{+}-u^{0})^{2}]$$

where g is defined as in (1.2).

Here one may select $u^{\pm}$ as the solution of the elliptic equations (1.8). However, as mentioned earlier, the solution of (1.8) shows some drawbacks.

We note that the level set function in the gradient-based model (1.1) evolves depending on the local profile of the edge detector $g = g(\nabla u^{0})$. Thus on should guess well initial values of the level set function. It is otherwise

often the case that the model fails to detect the desired boundaries. It is also known that the model can hardly find interior boundaries or contours that are very smooth or have discontinuous boundaries [14, Ch.12]. Therefore, we may consider the model (2.1) as a variant of (1.1), with the forcing term in the right side introduced in order to eliminate/minimize such drawbacks.

On the other hand, the MSCV model (1.7)-(1.8) shows a certain degree of global properties to overcome some drawbacks of (1.1); however, the computation of $u^{\pm}$ and their extension hardly make sense unless the image is essentially binary. The model is yet to be improved, e.g., by incorporating some of gradient information. In our new model, we suggest the replacement of the simple smoothing term (curvature) by a more reliable term that includes gradient information. Here we still have to answer the question: How to get $u^{\pm}$? See §4.2 below for an alternative solution for $u^{\pm}$.

2.2 Computational method for ϕ

Now we present a time-stepping procedure for (2.1): an incomplete backward Euler discretization combined with the alternating direction implicit (ADI) perturbation.

Let us assume that the values of ϕ at $t = t^{n-1}, \phi^{n-1}$, have been computed or initialized and that $u^{\pm}$ be updated. To obtain ϕ^n, consider the following incomplete backward Euler method for (2.1):

$$\frac{\phi^n - \phi^{n-1}}{\Delta t} - \alpha \mid \nabla_h \phi^{n-1} \mid \nabla_{h/2} \cdot \left(g \frac{\nabla_{h/2} \phi^n}{\mid \nabla_h \phi^{n-1} \mid} \right) = \beta \delta_\varepsilon(\phi^{n-1})[(u^- - u^0)^2 - (u^+ - u^0)^2] \quad (2.2)$$

where h is the spatial grid size and ∇_h and $\nabla_{h/2}$ denote respectively the standard and half-interval central difference schemes for the gradient operator. Along the boundary $\partial\Omega$, one can apply the no-flux boundary condition or whatever appropriate.

Let $\nabla_{h/2} = (D_{x1}, D_{x2})^T$. Define two linear operators (tri-diagonal matrices) and the source vector as

$$A_\ell^{n-1}\phi^n := -\alpha \mid \nabla_h \phi^{n-1} \mid D_{x\ell} \cdot \left(g \frac{D_{x\ell}\phi^n}{\mid \nabla_h \phi^{n-1} \mid} \right), \ \ell = 1,2$$
$$F^{n-1} := \beta \delta_\varepsilon(\phi^{n-1})[(u^- - u^0)^2 - (u^+ - u^0)^2] \quad (2.3)$$

Then, (2.2) can be rewritten as

$$\frac{\phi^n - \phi^{n-1}}{\Delta t} + (A_1^{n-1} + A_2^{n-1})\phi^n = F^{n-1} \quad (2.4)$$

The associated ADI method, studied by Douglas and Rachford [8], is as follows:

$$(1 + \Delta t A_1^{n-1})\phi^* = \phi^{n-1} - \Delta t A_2^{n-1}\phi^{n-1} + \Delta t F^{n-1},$$
$$(1 + \Delta t A_2^{n-1})\phi^n = \phi^* + \Delta t A_2^{n-1}\phi^{n-1} \quad (2.5)$$

which we call the Euler-ADI in this article. It is easy to see that the Euler-ADI is an $O(\Delta t^2)$ perturbation of (3.4). In each half of the calculation, the matrix to be inverted is tridiagonal, so that the algorithm requires $O(N = n_t n_x n_y)$ flops, where $n_p (p = x, y, or\ t)$ is the number of points in the p-direction. The ADI method was first introduced in three papers [5, 7, 16] by Douglas, Peace-man, and Rachford. The original ADI method is an $O(\Delta t^2)$ perturbation of the Crank-Nicolson difference equation solving the heat equation in 2D. The extra error appearing in the operator splitting is called the splitting error. As variants, Dyakonov, Marchuk, and Yanenko [9, 12, 19, 20] studied the fractional step (FS) method and Weickert and his colleagues [17] introduced the additive operator splitting (AOS) method. Recently, Douglas and KIM [6] analyzed a unified approach for the ADI and FS methods in which both methods are second-order accurate and their splitting errors are in third-order in time when applied for linear parabolic problems.

III. The Method of Background Subtraction

We consider a cartoon image which shows a rectangle on an oscillatory back-ground. When

the MSCV method is applied for the image, it easily produces extra boundaries. Such extra boundaries have been observed from various experiments; the method assumes some smooth portions as parts of boundaries. It seems to us that the phenomenon is not independent from the claim in [3,4]: the method can detect smooth boundaries. However, the ability mentioned in the claim is not always advantageous for the segmentation of general images. In order for the method to become effective for images of general backgrounds, we will consider the method of background subtraction.

Let the image be decomposed as

$$u^0 = \tilde{u} + \delta u, \qquad (3.1)$$

where $\tilde{u}$ is a smooth component(the background) of the image.

To illustrate the method of background subtraction, we will see Figure 2. There, the background and the projection (δu) are depicted for a cartoon image u^0. As one can see from the figure, there seems to be a high probability that the segmentation algorithm can detect the boundaries for δu more effectively rather than for u^0 itself, provided that the background is smooth enough not to distract the edges. Here the problem is how to choose such a background.

There must be many ways for choices of the background. In this section, we suggest an effective strategy, which has been motivated from the multigrid (multi-resolution) method that is quite popular in scientific computing:

1. Select a coarse mesh $\{\Omega_{ij}\}$ for the image domain Ω. Each element Ω_{ij} in the coarse mesh contains $m_x \times m_y$ pixels of the image, for some m_x, $m_y \geq 1$.

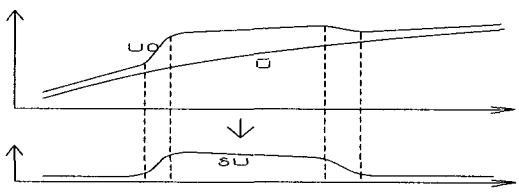

Figure 2. The method of background subtraction.

2. Choose a coarse image u_c on $\{\Omega_{ij}\}$:

$$u_{c,ij} = (a_{ij} + m_{ij})/2$$

where $u_{c,ij}$ denotes the value of u_c on Ω_{ij} and a_{ij} = the arithmetic average on Ω_{ij}, m_{ij} = the minimum on Ω_{ij}

3. Smooth u_c, with $u_c^{new} \leq u_c^{old}$ pointwisely.

For example, apply a few iterations of the modified five-point averaging described in (4.2) (the negative part) below.

4. Prolongate u_c to the original mesh Ω, for u_f One may apply the bilinear interpolation for the prolongation.
5. Smooth the prolongated image u_f. Apply a few iterations of a standard local averaging algorithm.
6. Assign the result for $\tilde{u}$.

In the above algorithm for the computation of $\tilde{u}$, one should determine parameters: the element size of the coarse mesh $(m_x \text{ and } m_y)$ and the iteration numbers for the smoothing algorithms of u_c and u_f. The automatic determination of such parameters is an interesting research task. It is apparent that the number of smoothing iterations depends on the element size of the coarse mesh. In this paper, we will select them experimentally; strategies for the automatic determination will appear separately along with various methods for the choice of the coarse image u_c.

IV. Acceleration Techniques

Efficiency can be a crucial factor for some applications. To improve the convergence speed for the detection of boundaries, one may consider strategies:

- an accurate initial guess for ϕ,

- a better solution for $u^{\pm}$, and
- an appropriate manipulation of ϕ during the iteration.

In the following, we present the strategies in detail.

4.1 Initial guess for ϕ

We may begin with a binary image u^0, i.e., u^0 contains two different values, say, 0 and 1. In the case, one can select the initial value of ϕ, ϕ^0, as follows:

$$\phi^0 = u^0 - \bar{u}^0 \tag{4.1}$$

where $\bar{u}^0$ is the ℓ^2 average of u^0.

Note that for simple binary images, the above initial value ϕ^0 is already able to locate the edges quite accurately.

For more general images, we would better apply the method of background subtraction and get $\delta u = u^0 - \tilde{u}$. Then, we can initialize ϕ as in (4.1), replacing u^0 by δu, for a faster convergence of the Euler-ADI iteration (2.5).

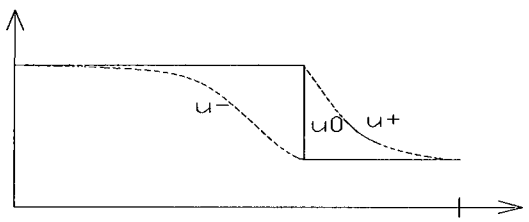

Figure 3. The original image u^0 and smooth images for $u^{\pm}$

4.2 An alternative solution for $u^{\pm}$

In this subsection, we will consider an alternative way of getting the CF which is much easier to simulate and makes sense for most cases having no triple junctions. Here the rule of thumb is that $u^{\pm}$ must be computed such that the difference between their average and the image u^0 should be able to introduce a reliable driving force for the evolution of the level set function.

See first Figure 3, where the original image u^0 and smooth images for $u^{\pm}$ are depicted. Such $u^{\pm}$ can be obtained utilizing one of various smoothing algorithms.

For example, one can apply a few iterations of modified five-point averaging:

$$u_{ij}^{\pm,k+1/2} = \left(u_{i-1,j}^{\pm,k} + u_{i+1,j}^{\pm,k} + u_{i,j-1}^{\pm,k} + u_{i,j+1}^{\pm,k}\right)/4$$
$$u_{ij}^{\pm,k+1} = \pm \max\left(\pm u_{ij}^{0},\ \pm u_{ij}^{\pm,k+1/2}\right) \tag{4.2}$$

Note that -max (-a, -b) = min(a, b)

As one can see roughly from Figure 3, quantity $u^0 - \frac{u^+ + u^-}{2}$ crosses zero near the desired edges and therefore it provides a driving force such that the level set function grows positively on one side of the edge and negatively on the other side. The above strategy can be suited well for many cases e.g., the detection of isolated objects, whether the edges are clear or not.

4.3 Modification of the level set function

For a quick response of ϕ to the driving force, it is natural to restrict the values of ϕ to be near zero, by imposing upper and lower limits. For example, when $\phi_{max} > 0$ denotes the desired maximum value, the adjusted level set function can be defined as

$$\widehat{\Phi}_{ij} = \Phi_{max} \cdot \frac{2}{\pi} \tan^{-1}(\Phi_{ij}) \tag{4.3}$$

Note that the right side is a smooth, symmetric, and increasing function, having the values in $(-\phi_{max}, \phi_{max})$.

V. Numerical Experiments

For numerical experiment, we choose gray scale images in public domain. In figure 3, we present the numerical results carried out utilizing

the gray scale house image in 256×256 cells. The original image, in figure 3(a), is segmented by MSCV model, as shown in figure 3(b). The original image is segmented by the proposed hybrid level set model in this paper, as shown in figure 3(c). As you see in figure, when the gradient method is implemented with appropriate hybrid level

set model, it work better than the conventional method. On the other hand, the segmented result in figure 4 also confirms that the new hybrid level method in this paper works better than the conventional MSCV method.

(a) (b)

(c)

Figure 3 Gray scale house images in 256X256 cells: (a) the original image, (b) the segment result using MSCV model, (c) the segment result by new proposed hybrid level set model

(a) (b)

(c)

Figure 4. Gray scale Lenna images in 256X256 cells: (a) the original image, (b) the segment result using MSCV model, (c) the segment result by new proposed hybrid level set model

Figure 5 shows the internal organs for human body. For experiment, the corpse is cool down in a refrigerating machine.

The refrigerated dead body is amputated at regular 3mm intervals by CNC Machine. The figure 5 shows a breast slice among the amputated slices. As one can see from top figure 5(a), the viscera below the lungs has complicated features, also has the triple junction. Furthermore, the gray level between viscera varies smooth. We call the phenomena to smoothing interface. As you see in figure 5(b), the conventional MSCV model misses most of these smoothing interfaces. However, the new proposed hybrid level set method segments most of smoothing interface except several case.

In last example shows that the hybrid level set segmentation algorithm can introduce non physical results, as other method so. Such non physical results have observed, showing various non physical segmentation, for about 5% of the given image. To overcome such difficulties, we may have to one or all of the following:

- 3D simulation: The missing portions of boundaries seem to be random. That is, a slice has little relation to adjacent ones for missing parts of boundaries. Thus it is natural to except from the observation that missing portions can be less sensitive in the 3D simulation than in 2D.
- Preprocessing: We may apply a set of preprocessing, in particular, noise removal and histogram transformation. These

techniques may alter the cartoon images.

VII. Conclusions

We have considered efficient and reliable numerical methods for PDE-based segmentation applied to house, lena, and CT scan images.

The article begins with preliminaries for the Mumford-Shah minimization problem in segmentation and level set formulation by Chan-Vese.

A backward Euler ADI procedure has been introduced for an efficient integration of Euler-Lagrange equations.

Futhermore, a new model is introduced by hybridizing level set formulation and complementary smooth function in order to smooth the driving force. The role of thumb is that CF must be computed such that the difference between their average and the original CF should be able to introduce a reliable driving force for the evolution of the level set function.

Also, to enhance the convergence speed, we have suggested two of new speed-up techniques: image dependent initialization and the imposition of an upper bound for level set function.

Numerical experiments has shown our hybrid algorithm can locate the zero-level set(segmentation) efficiently and reliably.

However, our algorithm also have shown drawbacks as other methods, when triple junction occurs. To overcome this drawback, we may have to introduce 3D simulation, and some of preprocessing $u^{\pm}$ so that the level set function can locate the zero level set at different locations.

(a)

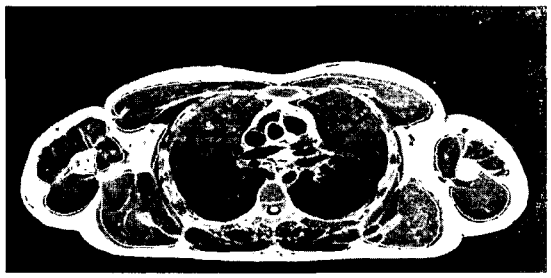

(b)

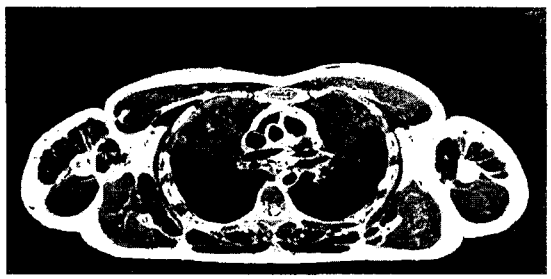

(c)

Figure 5 Gray scale internal organ images in 256x256 cells: (a) the original image, (b) the segmented result using MSCV model, (c) the segmented result by new proposed hybrid level set model

References

[1] V. CASELLES, F. CATTE, T. COLL, AND F. DIBOS, A geometric model for active contours in image processing, Numer Math., 66 (1993), pp. 1-31.

[2] V. CASELLES, R. KIMMEL, AND G. SAPIRO, Geodesic active contours, Int. J. Comput. Vision, 22 (1997), pp. 61-79.

[3] T. CHAN AND L. VESE, Active contours without edges, IEEE Trans. Image Process., 10 (2001), pp. 266-277

[4] A level set algorithm for minimizing the Mumford-Shah functional in image processing, in IEEE/Comput. Soc. Proc. of the First IEEE Workshop on Variational and Level Set Methods in Computer Vision, 2001, pp. 161-168.

[5] J. DOUGLAS, JR., On the numerical

integration of $\frac{\partial^2 u}{\partial x^2} + \frac{\partial^2 u}{\partial y^2} = \frac{\partial u}{\partial t}$ by implicit methods, J. Soc. Indust. Appl. Math., 3 (1955), pp. 42-65.

[6] J. DOUGLAS, JR. AND S. KIM, Improved accuracy for locally on-dimensional methods for parabolic equations, Mathematical Models and Methods in Applied Sciences, 11 (2001), pp. 1563-1579.

[7] J. DOUGLAS, JR. AND D. PEACEMAN, Numerical solution of two-dimensional heat flow problems, American Institute of Chemical Engineering Journal, 1 (1955), pp. 505-512

[8] J. DOUGLAS, JR. AND H. RACHFORD, On the numerical solution of heat con-duction problems in two and three space variables, Transaction of the American Mathematical Society, 82 (1960), pp. 421-439

[9] E. D'YAKONOV, Difference schemes with split operators for multidimensional unsteady problems (English translation), USSR Comp. Math., 3 (1963), pp. 581-607.

[10] M. KASS, A. WITKIN, AND D. TERZOPOULOS, Snakes: Acitive contour models, Int. J. Comput. Vision, 1 (1988), pp. 321-331.

[11] S. KICHENASSAMY, A. KUMAR, P. OLIVER, A. TANNENBAUM, AND A. YEZZI, Conformal curvature flows: From phase transitions to active vusion, Archive for Rational Mech, and Anal., 134 (1996), pp. 275-301.

[12] G. MARCHUK, Methods of numerical mathematics, Springer-Verlag, New York, Heidelberg, and Berlin, 1982.

[13] D. MUMFORD AND J. SHAH, Optimal approximation by piecewise smooth functions and associated variational problems, Comm. Pure Appl. Math., 42 (1989), pp. 577-685.

[14] S. OSHER AND R. FEDKIW, Level Set Methods and Dynamic Implicit Surfaces, Springer-Verlag, New York, 2003.

[15] S. OSHER AND J. SETHIAN, Fronts propagating with curvature dependent speed: algorithms based on Hamilton-Jacobi formulations, J. Comp. Phys,. 79 (1988), pp. 12-49

[16] D. PEACEMAN AND H. RACHFORD, The numerical solution of parabolic and elliptic equations, J. Soc. Indust. Appl. Math., 3 (1955), pp. 28-41.

[17] J. WEICKERT, B. TER HAAR ROMENY, AND M. VIERGEVER, Efficient and re-liable schemes for nonlinear diffusion filtering, IEEE Trans. on Image Processing , 7 (1998), pp. 398-410.

[18] R. WEINSTOCK, Calculus of Variations, Dover Publications, Inc., New York. 1974.

[19] N. YANENKO, Convergence of the method of splitting for the heat conduction equations with variable coefficients (English translation), USSR Comp. Math., 3 (1963), pp. 1094-1100.

[20] The method of fractional steps, Springer-Verlag, Berlin, Heidelberg, and New York, 1971. (English translation; originally published in Russian, 1967).

[21] H.-K. ZHAO, T. CHAN, B. MERRIMAN, AND S. OSHER, A variational level set approach to multiphase motion, J. Comput. Phys., 127 (1996), pp. 179-195.

[17] J. WEICKERT, B. TER HAAR ROMENY, AND M. VIERGEVER, Efficient and re-liable schemes for nonlinear diffusion filtering, IEEE Trans. on Image Processing , 7 (1998), pp. 398-410.

[18] R. WEINSTOCK, Calculus of Variations, Dover Publications, Inc., New York. 1974.

[19] N. YANENKO, Convergence of the method of splitting for the heat conduction equations with variable coefficients (English translation), USSR Comp. Math., 3 (1963), pp. 1094-1100.

[20] The method of fractional steps, Springer-Verlag, Berlin, Heidelberg, and New York, 1971. (English translation; originally published in Russian, 1967).

[21] H.-K. ZHAO, T. CHAN, B. MERRIMAN, AND S. OSHER, A variational level set approach to multiphase motion, J. Comput.

Phys., 127 (1996), pp. 179-195.

저자소개

주기세(Ki-See Joo)

1988년 한양대학교 산업공학과 (학사)
1992년 Texas A&M Univ. 산업공학과(석사)
1996년 고려대학교 산업공학과 (박사)
※관심분야 : 로봇비젼, 공장자동화, 3차원그래픽

김은석(Eun-Seok Kim)

1999년 대불대학교 산업공학과 (학사)
2001년 목포해양대학교 해양정보통신(석사)
2003년 아주대학교 산업공학과 (박사수료)
※관심분야 : Machine Vision, 3차원 그래픽